Chapter 5

Morphology Development in HDPE/Copolymer Blends: Quiescent and Flow-Induced Crystallization

5.1 INTRODUCTION

Due to their flexibility and toughness, materials containing short-chain branches (SCB) have found a significant niche in the plastics industry to make products, such as films having high tensile strength, impact and puncture resistance. The most common material used for these applications is linear low density polyethylene (LLDPE), which is typically either a heterogeneous or homogeneous ethylene copolymer depending on the catalyst used for its synthesis (Ziegler-Natta or metallocene, respectively).[1, 2]

The development of single-site metallocene catalyst has allowed for large-scale production of relatively well-defined ethylene/α-olefin copolymers with narrow molecular weight distributions and uniform SCB distribution.[3-8] Therefore, a great deal of effort has been put forth to understand crystallization behavior of these systems (e.g., studies in Chapter 3 on model SCB-containing materials) and achieve control over their physical properties.[9-19] Short-chain-branched systems exhibit strong changes in morphology compared to un-branched samples due to the exclusion of the short-chain branches from the crystalline phase.[19-24] The resulting decreased crystallinity leads to increased toughness and flexibility of the final material, prompting a number of studies of copolymer blends.[18, 25-27] Additionally, the presence of these chain defects results in a significant decrease in the response of the materials to flow without enhancement of crystallization kinetics or oriented morphology (see thesis Appendix B). This observation can be explained by either (1) the material’s inability to form oriented nuclei that lead to an increased nucleation density and template oriented growth or (2) the material’s inability to effectively propagate growth from an oriented nuclei.

To further examine these possibilities, we examine flow-induced crystallization (FIC) of a metallocene ethylene copolymer spiked with small amounts of high density polyethylene (HDPE) in order to promote oriented nuclei formation. The low concentration of a high-molecular-weight (slow-relaxing) HDPE ensures that the blend exhibits melt dynamics that are dominated by the fast-relaxing matrix, such that the few HDPE chains present are oriented by flow and form thread-like nuclei (Figure 5.1). In this way, we can evaluate the copolymer's ability to propagate an oriented morphology.

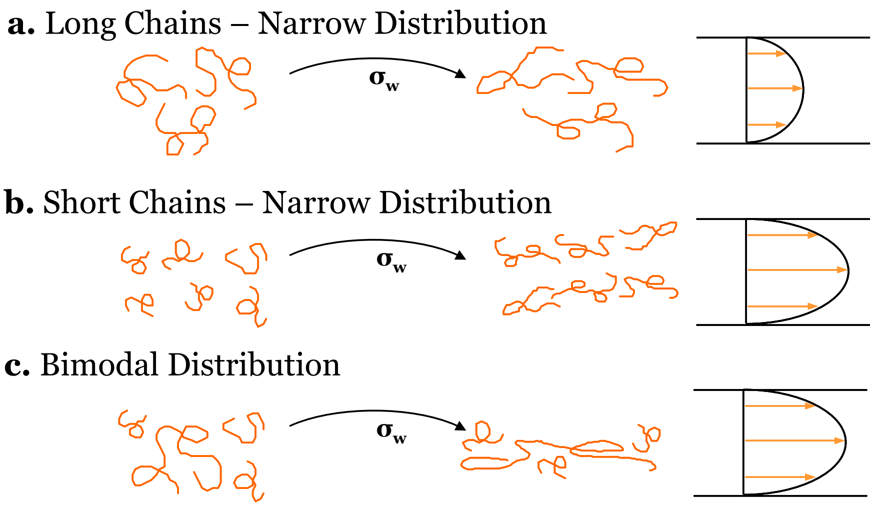

Figure 5.1 Schematic representation of the orientation of molecules by shear. **a)** Blends containing only long (slow-relaxing) chains undergo a small strain. **b)** Blends containing only short (fast-relaxing) chains undergo a large strain, but does not exhibit increased orientation compared to **a**. **c)** Blends containing a small amount of long chains in a predominately short-chain matrix exhibit melt dynamics dictated by the matrix (large strain) such that the slow-relaxing species is oriented by flow.

Recent studies of similar systems have observed the nucleation of polyethylenes having lower density or molecular weight by higher density or molecular weight polyethylene.[28-30] Increased crystallization kinetics and sample clarity were observed. These effects are further examined here both under quiescent conditions and subsequent to flow.

5.2 EXPERIMENTAL METHODS

5.2.1 Materials

Bimodal blends examined here consisted of a minor component of high density polyethylene (HDPE) having high molecular weight (M_w) and polydispersity (PDI = M_w/M_n) of 3.0. The major component was a fast-relaxing—but still entangled ($M_e \sim 1000$ g/mol)[31]—random ethylene copolymer (EH50) with a melt index (MI) of 16.5 g/10 min. This metallocene-catalyzed copolymer having approximately 5 mol % hexene was selected to mimic the SCB content of the series of hydrogenated polybutadienes (HPBDs) outlined in Chapter 3. One of these HPBDs, L53, is included for comparison in Table 5.1, which outlines the molecular characteristics of the bimodal blend components. EH50 was graciously provided and characterized by Dr. David Lohse and his team (ExxonMobil, Clinton, NJ) and the HDPE sample by Chevron Phillips.

Table 5.1 Molecular characteristics of polyethylene materials.

Polymer	Type	M_w (kg/mol)	PDI	SCB/ 1000 back-bone C[a]	T_m (°C)[d]
EH50[b]	Linear	50	2.9	25.7	96
HDPE[c]	Linear	529	3.0	0.2	136
L53[b*]	Linear	53	<1.05	19.2	110

[a] obtained via ^{13}C NMR
[b] corresponding values provided by ExxonMobil
[c] corresponding values provided by Chevron Phillips
[d] peak temperature as determined by DSC during ramps at 10 °C/min
[*] not examined in current studies

Blends containing a small concentration of HDPE in EH50 were made via solution blending. This blending procedure results in homogeneous mixtures and avoids problems encountered in melt extrusion blending,[32] such as long-chain degradation and incomplete mixing due to viscosity differences between the two components. Both polymers were dissolved in 1,2,4-trimethylbenzene at 130 °C along with approximately 30 mg of antioxidant, butylated hydroxytoluene (BHT). The solutions were precipitated in an excess (8:1) of cold methanol, and there resulting participates were filtered and dried in a vacuum oven for one week at 60 °C. Low HDPE concentrations were selected in order to minimize crystallization-induced phase separation. Concentrations on either side of the HDPE overlap concentration, c^*, were selected. The overlap concentration is defined as the concentration at which the corresponding chains just pervade all volume (see Figure B.1) and thus depends upon the radius of gyration (R_g) and molecular weight (M_w) of chains:

$$c^* = \frac{3M_w}{4\pi R_g^3 \rho N_a}, \tag{5.1}$$

where N_a is Avogadro's number (6.022×10^{23}) and ρ is density.[33, 34] From small-angle neutron scattering measurements, R_g (Å) of melt-crystallized linear polyethylene was found to depend on M_w (g/mol) as[35, 36]

$$R_g = (0.45 \pm 0.01)M_w^{1/2}. \tag{5.2}$$

Using a density of 0.95 g/cm^3, eqs 5.1 and 5.2 yield $c^* \approx 0.6\%$. Hence, blends containing 0%, 0.25%, 0.5%, 0.75%, 1% and 5% HDPE by weight were examined.

5.2.2 Differential Scanning Calorimetry

Differential Scanning Calorimetry (DSC) experiments were conducted by Dr. Soo-Young Park (Kyunpook National University, Daegu, South Korea) to study nucleation in HDPE blends (5-10 mg samples) using a Perkin Elmer 7 DSC system calibrated with an indium standard. Both temperature ramps and isothermal studies were conducted under a nitrogen atmosphere. Temperature ramps were conducted at 10 °C/min from 160 °C to 40 °C to obtain peak melting and crystallization temperatures (T_m and T_x, respectively).

Nucleation studies examined the effect of hold-time (t_{hold}) at elevated temperatures on subsequent crystallization rates at lower temperature; at the elevated temperature negligible crystallization of EH50 (major component) occurs while HDPE (minor component) is highly supercooled. Samples containing 0, 0.5, and 1 wt % HDPE were first heated to 160 °C and left for 5 minutes in order to erase thermal history. Samples were then cooled to the hold temperature (T_{hold}) of 100 °C or 105 °C at 40 °C/min where they were left for $0 \leq t_{hold} \leq 5$ min. Subsequently, samples were cooled to an isothermal crystallization temperature (T_c) of 90 °C at 40 °C/min and left to crystallize for 1 hour during which period heat flow was recorded as a function of time. Position of the peak in heat flow, t_{max}, was used as a measure of crystallization rate.

5.2.3 Flow-Induced Crystallization

Flow-induced crystallization (FIC) studies were conducted using a shear-stress-controlled instrument previously built and described by Kumaraswamy et al.[37] Briefly, a pneumatic actuator drove molten polymer into a rigid flow cell equipped with windows for in-situ monitoring of morphology development. For optical characterization, the quartz windows of the flow cell were replaced with low-birefringence BK7 windows (Foctek Photonics, Inc.). For x-ray characterization, diamond or beryllium windows were used. The flow channel is a rectangular slit with an aspect ratio greater than 10 in order to approximate a two-dimensional flow profile (width = 6.35mm, height = 0.5 mm, length =

63.5 mm). Assuming parallel-plate flow, the shear imposed on the sample varies linearly from its value at the wall (σ_w) to 0 at the center of the channel in the direction of the velocity gradient ($\nabla \mathbf{v}$). Minor alterations to the instrument included the use of compressed air and a re-circulating oil bath set to 0 °C in order to enable rapid cooling of the sample to the lower temperatures that are necessary for polyethylene (PE) compared to polypropylene, for which the instrument was initially designed.

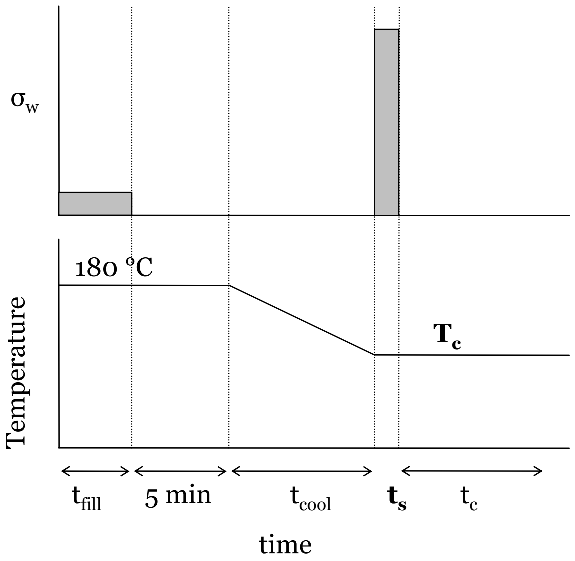

Figure 5.2 Experimental short-term shearing protocol.

Isothermal crystallization was examined following a short shear pulse based on a protocol developed by Janeschitz-Kriegl and co-workers (Figure 5.2).[38] Initially, the cell was filled with sample at 180 °C and low wall shear stress (t_{fill} = 25 s, $\sigma_w \sim 0.02$ MPa). The sample was maintained at this high temperature, which is above the equilibrium melting point of polyethylene (~ 145 °C)[39] for 5 min to ensure full erasure of the flow history. The cell was then cooled to the crystallization temperature, T_c, as quickly as possible; cooling times (t_{cool}) ranged between 8 and 15 min, with the large thermal mass of the instrument being the limiting factor in cooling rate. Isothermal crystallization was examined at T_c = 92, 95, and 98 °C. Once at T_c, the system temperature was maintained with the aid of a second re-circulating oil bath set to $T_c + 6$ °C. For FIC studies, upon reaching T_c, a pressure drop between 60 and 100 psi was applied across the flow cell (corresponding to 0.07 MPa $\leq \sigma_w \leq$ 0.14 MPa) for shearing times (t_s) ranging between 6 and 15 seconds. The amount of polymer extruded was limited to 110 mg to ensure that all material reaching the analysis window of the flow cell had the same flow and thermal histories.

5.2.4 Optical Characterization

Isothermal crystallization was followed in situ using optical and x-ray probes in the velocity gradient direction (Figure 5.3). A 632.8 mm He-Ne laser was employed for transmittance, apparent birefringence, and H_v (cross-polarized) small angle light scattering (SALS) measurements both during and following the shear pulse. Sample transmittance (I/I_0) is given by total intensity, I, normalized by the pre-shear total intensity, I_0, and can be used to monitor overall crystallization kinetics. Optical anisotropy of the sample is manifested in what we term the 'apparent' birefringence: $I_{perp}/I = I_{perp}/(I_{para} + I_{perp})$, where I_{perp} and I_{para} are the light intensity transmitted through crossed and parallel polarizers, respectively. This value is related to the birefringence by

$$\frac{I_{perp}}{I} = \sin^2\left(\frac{\pi d \Delta n}{\lambda}\right) = \sin^2\left(\frac{\delta}{2}\right), \tag{5.3}$$

where d is the sample thickness along the direction of light with wavelength λ = 632.8 nm, Δn is the birefringence averaged over the path length of the laser, and δ is the sample retardance.[40] SALS patterns in H_v polarization mode were recorded using a polarizer and analyzer oriented at +45° and -45° to vertical. These patterns were collected simultaneously with the other optical measurements by the use of a hole at the center of the analyzer that allows un-scattered light to pass through. SALS provides additional information regarding morphological superstructures developed during crystallization.

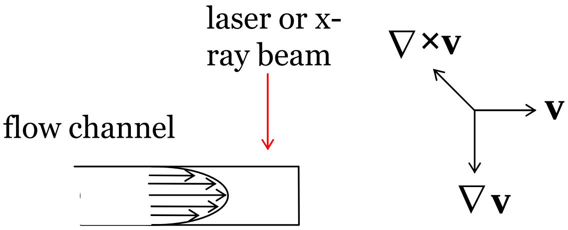

Figure 5.3 Schematic representation depicting coordinate axes relevant to flow experiment.

5.2.5 X-ray Scattering

Morphology development during quiescent crystallization and crystallization subsequent to flow was followed using wide and small angle x-ray scattering (WAXS and SAXS, respectively). WAXS was conducted at beamline X27C of the National Synchrotron Light Source (Brookhaven National Lab, Upton, NY).[41] A MARCCD detector with 158 μm pixel size was used to record two-dimensional scattering patterns generated with x-rays of wavelength, λ, of 1.371 Å. The camera length was calibrated using aluminum oxide (Al_2O_3). Thermal and flow history were controlled by the apparatus described above.

SAXS experiments were conducted at the DUBBLE beamline (BM26) at the European Synchrotron Radiation Facility (ESRF, Grenoble, France).[42] A multi-wire gas-filled detector with 260 μm pixel size was used to record two-dimensional scattering patterns generated with x-rays of wavelength, λ, of 1.03 Å. The sample-to-detector distance was calibrated using dry rattail collagen. Shear experiments were conducted using the apparatus described above. Additionally, quiescent crystallization was conducted at 95 and 98 °C using a Linkam Shear cell equipped with Kapton windows. The gap width was set to 500 μm to match the light path length in the flow apparatus described above.

X-ray data pre-treatment included the subtraction of a background and adjustment for incident flux and acquisition time. The azimuthally-averaged intensity, $I(q)$, was extracted as a function of scattering vector, $q = 4\pi\sin(\theta)/\lambda$, where θ is the scattering angle. For isotropic samples, a Lorentz correction was applied by multiplying the scattering intensity, $I(q)$, by the square of the scattering vector, q: $J(q) = I(q)q^2$.[43]

The area under the Lorentz-corrected SAXS intensity curve (for isotropic samples) for the full range of q ($0 < q < \infty$) defines the invariant, which is a measure of the total scattering power of the sample. Given the experimental constraints, we approximate the invariant by the integrated intensity, Q, in the range available ($q_{min} < q < q_{max}$):

$$Q = \int_{q_{\min}}^{q_{\max}} q^2 I(q) dq \; . \tag{5.4}$$

The evolution of this invariant can be used to examine relative crystallization kinetics and relative crystallinity in systems with similar electron density differences.

Wide angle x-ray scattering data proved difficult to analyze by conventional methods (peak fitting of amorphous halo and crystalline reflections)[44] due to the low crystallinity levels of the blends. Instead, the azimuthally-averaged intensity of the (110) reflection is used as an estimate of relative crystallinity. Crystallization rates could be compared by the autocorrelation intensity, A, of the (110) crystalline reflection during crystallization:

$$A(q_{110}) = \frac{1}{m-1}\sum_{i=1}^{m}\widetilde{I}(q_{110},t_i)\cdot\widetilde{I}(q_{110},t_i), \qquad (5.5)$$

where m is the total number of intensity curves, t_i corresponds to the time point of acquisition, and $\widetilde{I}(q,t_i)$ is the dynamic intensity defined as

$$\widetilde{I}(q,t_i) = I(q,t_i) - \frac{1}{m}\sum_{i=1}^{m} I(q,t_i). \qquad (5.6)$$

Alternatively, relative crystallinity and degree of orientation were examined using a differential analysis developed by Hajimorad et al.[45] In this analysis, the relative degree of crystallinity was measured by the peak intensity of the (110) reflection. A quantitative comparison of the degree of orientation was made using the normalized harmonic of the Fourier transform capturing the azimuthal dependence of the intensity (in our case, the second harmonic). These measurements were made for both overall scattering intensities and differential intensities. The latter were calculated by examining 2D scattering patterns relative to previous points in time. For example, data presented at t = 615 s were collected from a 2D image that was obtained by subtracting the 2D scattering pattern at the previous time point of t = 195 s from the 2D scattering image at t = 615 s after both were normalized to account for the incident beam flux and acquisition time.[45]

5.2.6 Scanning Transmission Electron Microscopy

Scanning transmission electron microscopy (STEM) images for EH50 and its blends containing 0.5, 0.75, and 5 wt % HDPE were obtained by Dr. John Stuyver and Dr. Anton-Jan Bons (ExxonMobil, Machelen, Belgium). These samples were isothermally crystallized at 98 °C for 30 minutes and subsequently cooled to room temperature at

40 °C/min in a Perkin Elmer 7 DSC system under nitrogen atmosphere. Images were obtained in high-angle annular dark field (HAADF) mode following staining with ruthenium tetroxide (RuO_4) and cryo-microtoming. Image contrast was inverted in order to be comparable with conventional transmission electron microscopy (TEM) bright field images.

5.3 RESULTS

5.3.1 Quiescent Crystallization

5.3.1.1 DSC Nucleation Studies

The addition of HDPE to EH50 resulted in a pronounced enhancement of crystallization kinetics (Figure 5.4). In these studies, we examined the peak crystallization time (t_{max}) for isothermal crystallization at 90 °C following a hold for a specified time, t_{hold}, at T_{hold} = 100 or 105 °C. The addition of even a small amount of HDPE (0.5 wt %) led to nearly a 5-fold increase in crystallization rate. At short hold times of 0 or 1 min, doubling the HDPE concentration from 0.5 to 1 wt % doubled the crystallization rate. Longer hold times led to greater enhancement of crystallization kinetics for the 1 wt % HDPE blend. When the samples were cooled stepwise with a 3-minute hold at 100 °C, the 1 wt % blend exhibited crystallization kinetics that were approximately 25 times faster compared to the 0.5 wt % blend. In contrast, the crystallization kinetics of the 0 and 0.5 wt % blends were not significantly affected by hold times of up to 5 minutes at elevated temperatures (i.e., similar t_{max} at different t_{hold}).

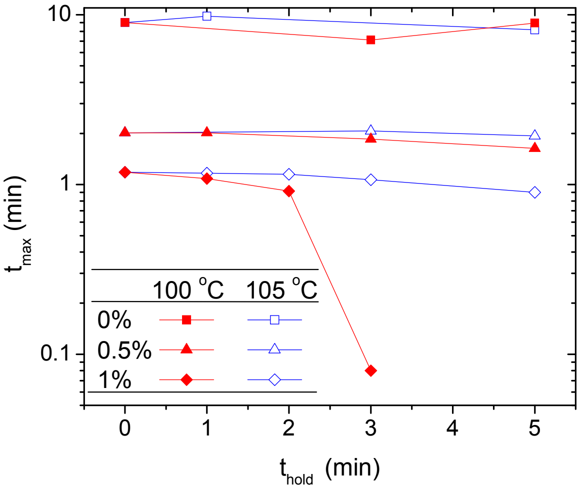

Figure 5.4 Time of peak crystallization (t_{max}) during 60 min at 90 °C as a function of hold time (t_{hold}) at 100 and 105 °C for 0, 0.5 and 1 wt % blends of HDPE in EH50.

5.3.1.2 Optical Characterization

Blends containing HDPE in EH50, even at the lowest concentration examined of 0.25 wt %, exhibited transmittance behavior that was qualitatively different from the ethylene-co-hexene base resin (Figure 5.5). Quiescent crystallization of EH50 containing 0 wt % HDPE exhibited a monotonic decrease in transmittance during crystallization at 98 °C following an induction period of approximately 10^3 s. In contrast, the three blends exhibited minima in transmittance evolution and subsequently maintained transmittance values above 50% on the same timescale. In previous studies, this minimum has been attributed to the half-filling of space by crystalline structures (i.e., when the size of the morphological features is on the order of the space between them).[46-50] The depth of the minima and their position in time followed a monotonic trend with HDPE concentration. Greater clarity both at the minimum in transmittance and during subsequent crystallization was observed with increasing HPDE content in the range examined; the 1 wt %

HDPE blend recovered to 96% transmittance. Additionally, the increase of turbidity (decrease of transmittance) with time and hence, crystallinity, reduced with increasing HPDE content. The nucleating effect of HDPE is apparent in the onset of the growth of turbidity which occurs at approximately 90 s for the 0.25% HDPE blend, 40 s for the 0.5% blend, and 10 s for the 1% blend.

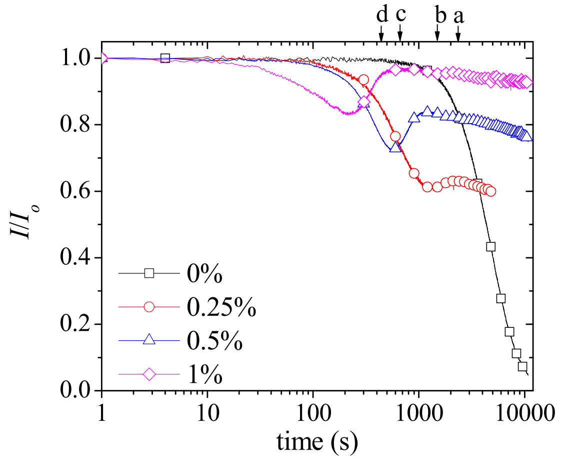

Figure 5.5 Transmittance (I/I_0) of HPDE blends crystallized quiescently at 98 °C. a, b, c, and d denote the times at which H_v SALS patterns (Figure 5.6) were collected for the 0, 0.25, 0.5 and 1 wt % blends, respectively.

The difference in optical behavior between EH50 and HDPE/EH50 blends is also apparent in 2D H_v SALS patterns (Figure 5.6). EH50 exhibited isotropic H_v SALS patterns corresponding to depolarization of light by randomly oriented scattering entities (Figure 5.6a). In contrast, HDPE/EH50 blends exhibited H_v SALS patterns with an azimuthal dependence that mimics 4-lobe patterns, which are usually associated with spherulite formation (Figure 5.6b-d).[51, 52] Even at the lowest concentration examined of 0.25 wt % HDPE, a faint 4-lobe pattern was observed (Figure 5.6b). The distorted 4-lobe SALS patterns apparent for 0.5 and 1 wt % HDPE blends (Figure 5.6c and d, respectively) are typically attributed to very poorly formed spherulites categorized as 'type-c' spherulites.[53]

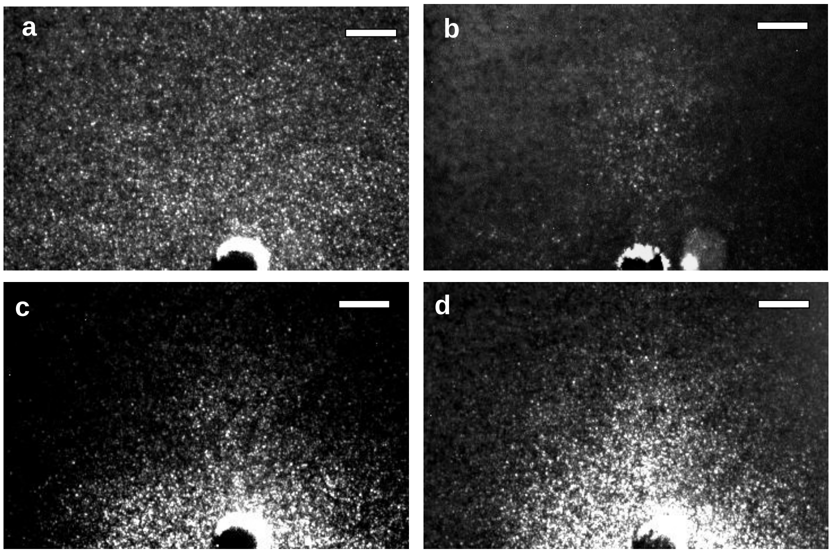

Figure 5.6 H_v SALS patterns of **a)** 0 wt %, **b)** 0.25 wt %, **c)** 0.5 wt %, and **d)** 1 wt % HDPE blends collected at time points indicated in Figure 5.5 during quiescent crystallization at 98 °C. Scale bar corresponds to $2\theta = 2°$.

Intensity and shape of H_v SALS patterns of HDPE/EH50 blends vary with position along the non-monotonic transmittance curve (Figure 5.7–5.9). With the apparatus used here, no scattering pattern could be recorded prior to the minimum in light transmittance (SALS images 1-3 in Figure 5.8 and half-filled symbols in Figure 5.9). Even the 0.25 wt % HDPE blend (not shown), whose minimum corresponded to 60% transmittance, exhibited only minor increases in overall H_v scattering power prior to the minimum (similar to Figure 5.9). Near the minimum in transmittance, a strong increase in H_v SALS intensity was observed (point 4 in Figure 5.7–5.9). The H_v SALS pattern (image 4 Figure 5.8) exhibited some azimuthal dependence (Figure 5.9), which became more pronounced as transmittance values increased (points 5-6 in Figure 5.7). A 4-lobe pattern was easily recognized in the range where transmittance resumed decreasing (points 7 and 8 in Figure 5.7–5.9). Furthermore, azimuthal dependence at long times ($>10^4$ s) revealed increased scattering both within and between the ‘lobes’ of the H_v SALS pattern (curve 8 in Figure 5.9). These observations are in agreement with prior studies of polyethylene crystallization.[49, 54]

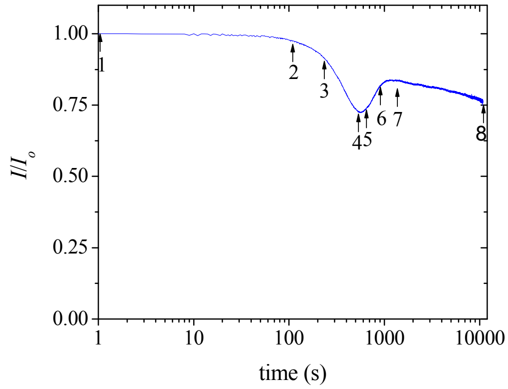

Figure 5.7 Transmittance of 0.5 wt % HPDE blend crystallized quiescently at 98 °C. Numbers mark time at which H_v SALS images (Figure 5.8) were collected.

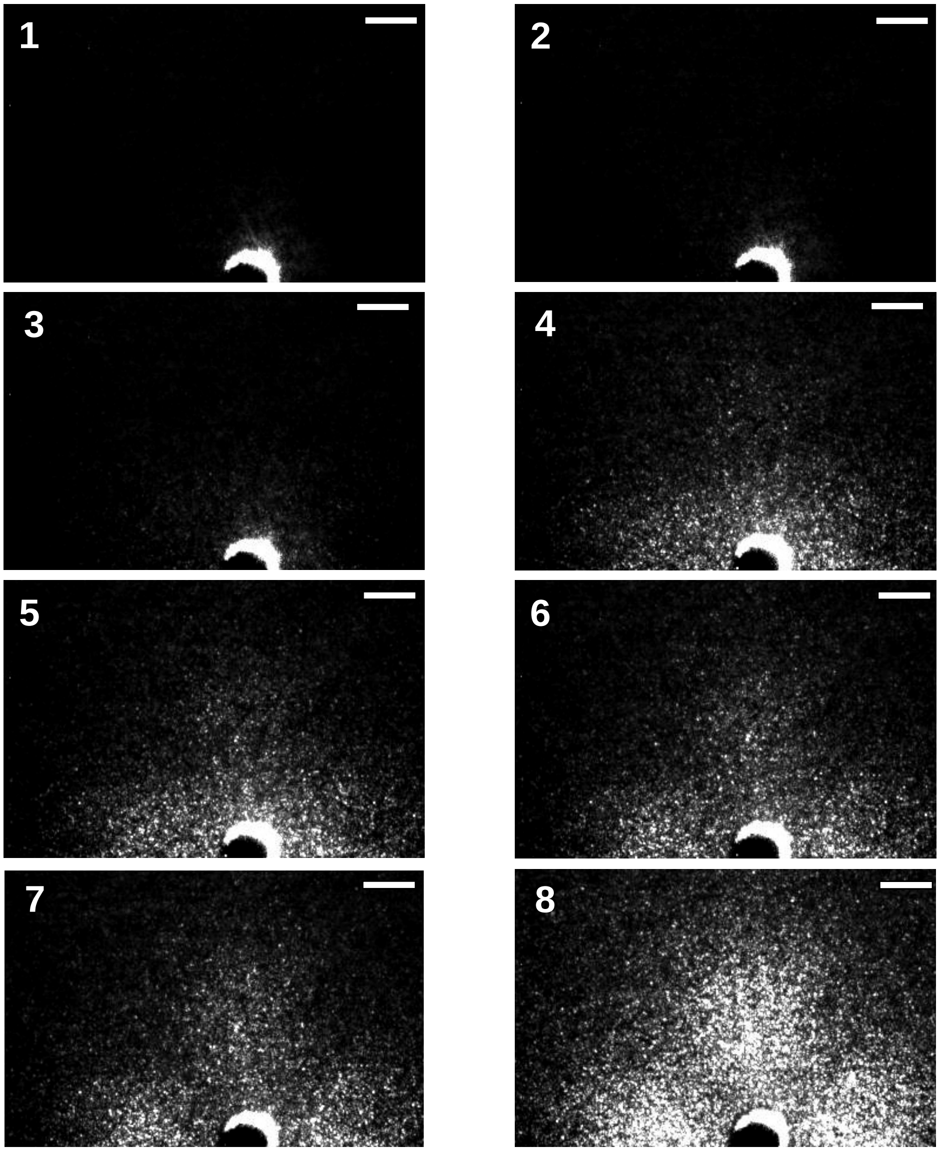

Figure 5.8 H_v SALS images of 0.5 wt % HPDE blend undergoing quiescent crystallization at 98 °C corresponding to points marked in transmittance curve (Figure 5.7). Scale bar corresponds to $2\theta = 2°$.

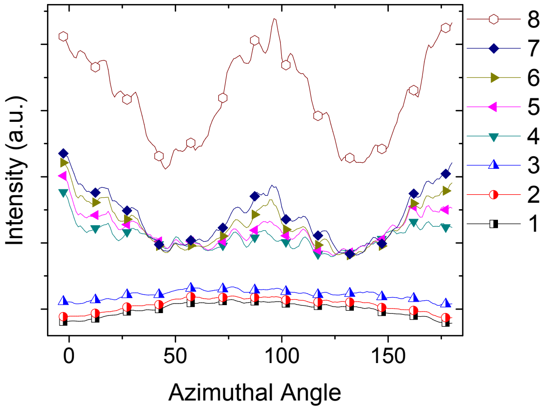

Figure 5.9 Azimuthal dependence of H_v SALS intensity in Figure 5.8 for 0.5 wt % HDPE blend quiescently crystallized at 98 °C at time points marked in Figure 5.7.

While there are similarities between these optical behaviors and those in previous studies,[49, 54] a very important distinction exists. Although 4-lobe H_v SALS images are predominately associated with spherulitic growth, polarized optical microscopy (POM) images indicated that hardly any spherulites form for the 0, 0.5, and 0.75 wt % blends (Figure 5.10).

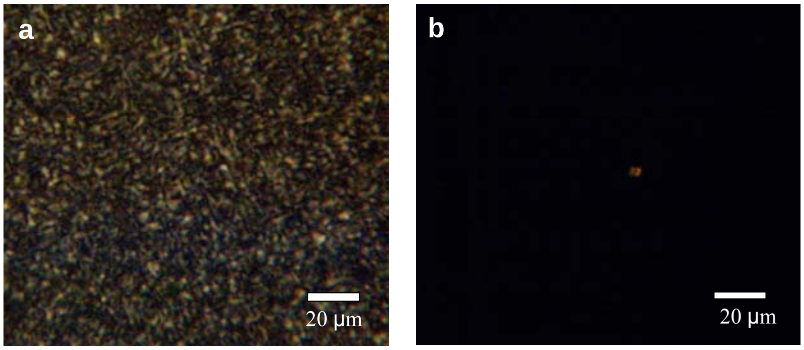

Figure 5.10 POM images of **a)** HDPE and **b)** 0.5 wt% HDPE/EH50 blend.

The nucleation effect of HDPE is also apparent in H_v scattering patterns at short crystallization times. In contrast to the 0.5 wt % HDPE blend, for which an induction period for the development of H_v scattering was observed, the 1 wt % HDPE blend exhibited an isotropic scattering pattern upon reaching the isothermal crystallization temperature of 98 °C (Figure 5.11; compare with image 1 in Figure 5.8), indicating crystallization of the blend during cooling. Analogous to the H_v pattern of the 5 wt % blend, that of the 1 wt % blend remained relatively unchanged up until the minimum in transmittance (Figure 5.5), at which point the scattering pattern developed azimuthal dependence. At long times (t ~ 10^4 s), a 4-lobe pattern emerged.

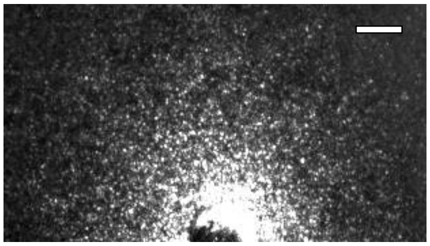

Figure 5.11 H_v SALS image of 1 wt % HDPE blend at the onset of isothermal crystallization at 98 °C (t = 0 s). Scale bar corresponds to $2\theta = 2°$.

5.3.1.3 X-ray Characterization

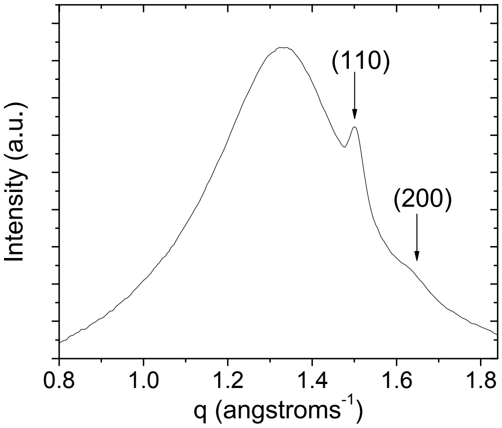

Figure 5.12 WAXS intensity of 1 wt % HDPE/EH50 blend after isothermal crystallization at 98 °C for 30 minutes with crystalline reflections as indicated.

Extremely low crystallinity levels at the elevated isothermal temperatures examined here present significant challenges to WAXS data processing. The (110) orthorhombic reflection consistently displayed lower intensity than the amorphous halo and the

(200) crystalline reflection was never resolved (Figure 5.12; compare with Figure 4.2 in Chapter 4). Peak fitting of the amorphous halo and the crystalline reflections was not successful, and hence, a crystallinity index could not be evaluated. Alternatively, the peak intensity of the (110) crystalline reflection was used to gauge the relative amount of crystallinity. Relative crystallization rates could be compared via the autocorrelation intensity, $A(q_{110})$, of the (110) crystalline reflection (eqs 5.5 and 5.6), which is a measure of the overall rate of change of intensity at a given q-value, and hence the rate of crystallization. Crystallization rates were observed to increase with HDPE concentration (Table 5.2), and furthermore, the significant difference between the rates of change of the 0.75 and 1 wt % blends suggests that the overlap concentration for HDPE lies between these two concentrations ($0.75 < c^* < 1$).

Table 5.2 Autocorrelation intensities of (110) reflections during isothermal crystallization of HDPE/EH50 blends.

% HDPE	T_c = 95 °C ($\times10^{-4}$)	T_c = 98 °C ($\times10^{-4}$)
0.25%		2
0.5%	1	5
0.75%	4	7
1%	30	

Small angle x-ray scattering of the 0, 0.5 and 0.75 wt % blends during isothermal crystallization at 98 °C (and 95 °C, not shown) revealed an overall increase in scattering power of the blends (Figure 5.13a). This behavior is similar to that of a hydrogenated polybutadiene undergoing isothermal crystallization at a high temperature that was observed in Chapter 3 (Figure 3.15a); a decrease of scattering intensity at low q was not observed, indicating that morphology development was dominated by growth of primary lamellae. The SAXS integrated intensity revealed increased crystallinity and confirmed increased crystallization rate with greater HDPE content (Figure 5.13b).

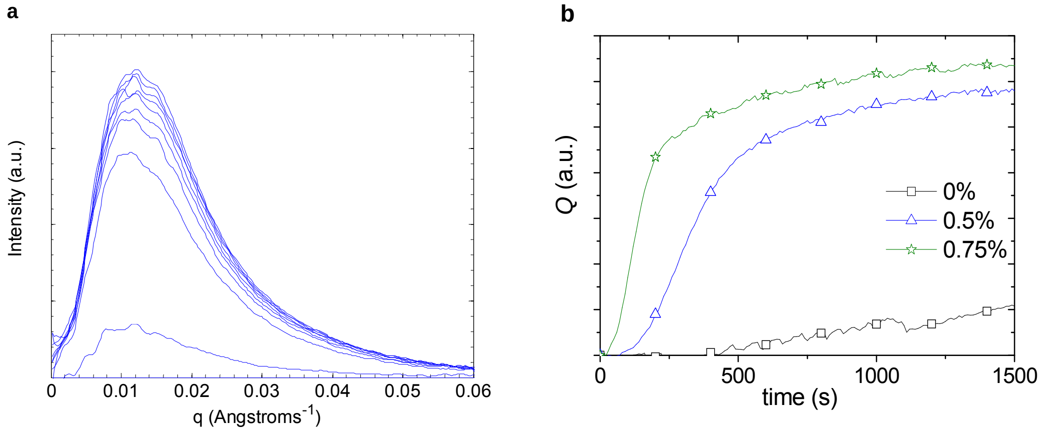

Figure 5.13 a) Evolution of SAXS intensity, $I(q)$, for 0.75 wt % HDPE blend during quiescent crystallization at 98 °C. **b)** Relative SAXS integrated intensity (Q) for different HDPE/EH50 blends during quiescent, isothermal crystallization at 98 °C.

5.3.1.4 STEM Images

STEM images obtained for samples crystallized at 98 °C for 30 minutes and subsequently cooled to room temperature at 40 °C/min underscore the pronounced effect of HDPE on the morphology of copolymer systems (Figure 5.14). EH50 alone was found to consist of short, randomly oriented lamellae (Figure 5.14a). On the other hand, an addition of HDPE at concentrations even below its overlap concentration (c = 0.5 wt % < c^*) resulted in a significant increase in length and local orientation of the lamellae (Figure 5.14b). The 5 wt % HDPE blend (c ~ 10 × c*) exhibited evidence of phase separation (Figure 5.14c), showing thicker lamellae compared with 0.5 wt % HDPE blend embedded in the fine-grained, randomly oriented morphology characteristic of pure EH50 (Figure 5.14a). No evidence of spherulitic growth was observed.

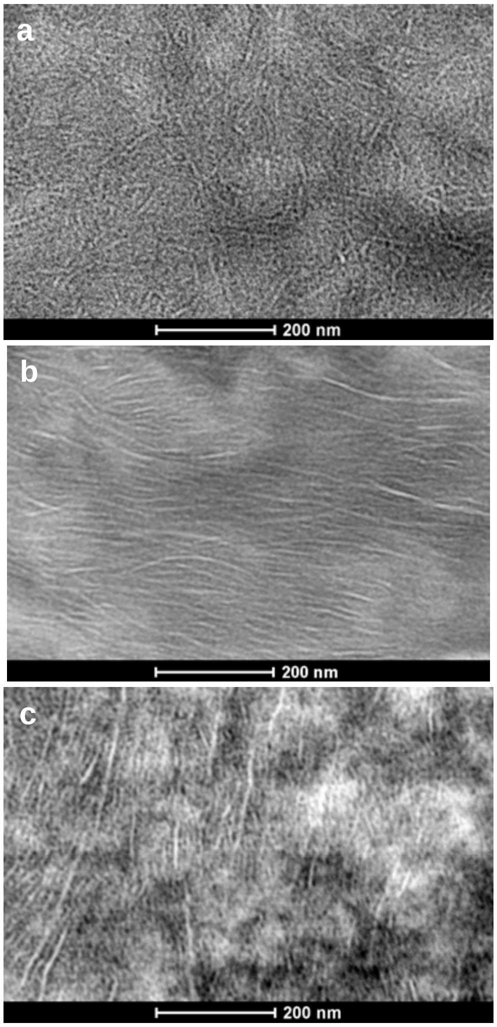

Figure 5.14 STEM images of **a)** EH50, **b)** 0.5 wt % HDPE blend, and **c)** 5 wt % HDPE blend subsequent to crystallization at 98 °C for 30 min and cooling to room temperature.

5.3.2 Flow-Induced Crystallization

5.3.2.1 Optical Characterization

The clarifying effect observed under quiescent conditions was also observed following the imposition of shear (Figure 5.15a). Similar to the quiescent case, transmittance for both the 0 and 0.5 wt % blends subsequent to shear decreased to a local minimum; however, relative to the quiescent case, these minima were shallower and, for the 1 wt % blend, occur at earlier time (no significant difference for 0.5 wt % blend). In contrast to quiescent conditions (Figure 5.5), both 0.5 and 1 wt % HDPE blends produced equally transparent microstructures (Figure 5.15a, t > 500 s). Relative to the quiescent case, short-term shearing improved the transmittance of the 0.5 wt % blend and decreased the transmittance of the 1 wt % blend. These opposite trends may be related to the increase in transmittance and oriented structure formation of the 1 wt % blend.

The 1 wt % HDPE blend exhibited an increase in transmittance during shear above its initial value at the start of the experiment (t = 0 s when T = 98 °C). This value, I/I_0(t = 0) was below 1.0 because crystallization during cooling (t_{cool} region in Figure 5.15a) resulted in the formation of scattering entities. Upon shear (t_s region in Figure 5.15a), sample transmittance was almost fully restored.

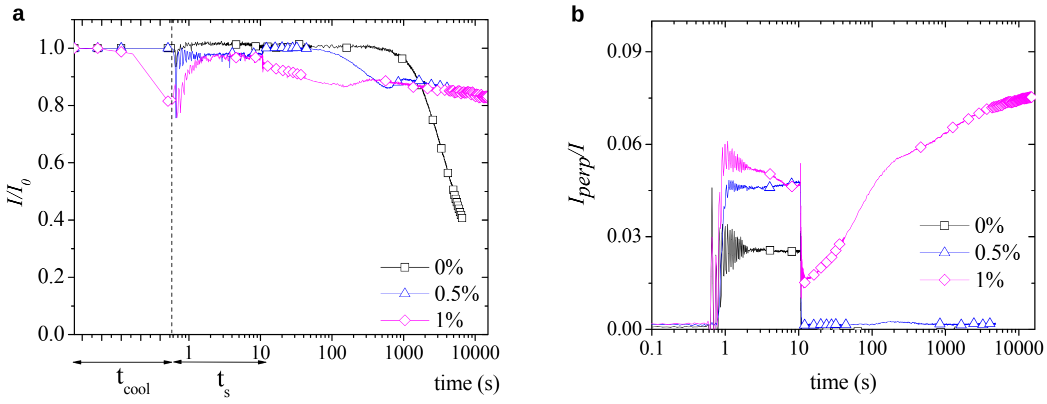

Figure 5.15 a) Transmittance and **b)** corresponding apparent birefringence of HDPE/EH50 blends during and subsequent to shear at 98 °C, $\sigma_w = 0.14$ MPa for $t_s = 10$s. **a** includes transmittance during cooling (t_{cool}) on a linear timescale occurring over 9 min.

Apparent birefringence (I_{perp}/I) revealed no orientation for blends having HDPE concentration below overlap ($c < c^*$) and surprisingly little orientation for the 1 wt % HDPE ($c > c^*$; Figure 5.15b). The non-zero value of I_{perp}/I at the cessation of shear (t =

10 s) exhibited by the 1 wt % HDPE blend indicates the presence of oriented structures. The largest apparent birefringence values reached at long times subsequent to shear were not much greater than melt birefringence during flow. This represents a stark contrast to prior literature on bimodal blends with a small concentration of long chains in a matrix of chain that have similar very low chain defect content (i.e., stereo-errors in isotactic polypropylene, iPP, or comonomer in PE) has shown that the creation of oriented structures during flow templates highly oriented growth after cessation of flow.[38, 46, 55-57] In these pervious systems, the birefringence often increases much more than ten times relative to the birefringence that remains after cessation of shear. Additionally, the shape of the birefringence curve at long time is dissimilar to highly crystalline systems undergoing FIC (e.g., Figure B.3 in thesis Appendix B). Highly oriented growth is generally characterized by rapidly increasing I_{perp}/I subsequent to shear with a rate of change that increases with time as oriented structures propagate; the slope, dI_{perp}/dt, only decreases when the sample retardance, δ, approaches $\pi/2$ due to its sinusoidal dependence.[56] In contrast, at approximately 200 s, the apparent birefringence of the 1 wt % HDPE shows a distinct decrease in slope even though $\delta \ll 1$; this decreases in slope was apparent for all samples displaying non-zero birefringence following shear.

H_v SALS images confirmed mild oriented growth in both blends. Similar to quiescent crystallization, the 0.5 wt % blend did not exhibit H_v scattering until after an induction period of approximately 420 s. At this point, a very light streak normal to the shear direction could be observed corresponding to long, slender scattering objects aligned parallel to the flow direction.[52, 58, 59] This streak persisted for a short time (less than 480 s) after which a very light 4-lobe pattern could be observed. The 1 wt % blend exhibited both a streak and isotropic scattering immediately following shear. As time progressed, this streak became dominated by isotropic scattering.

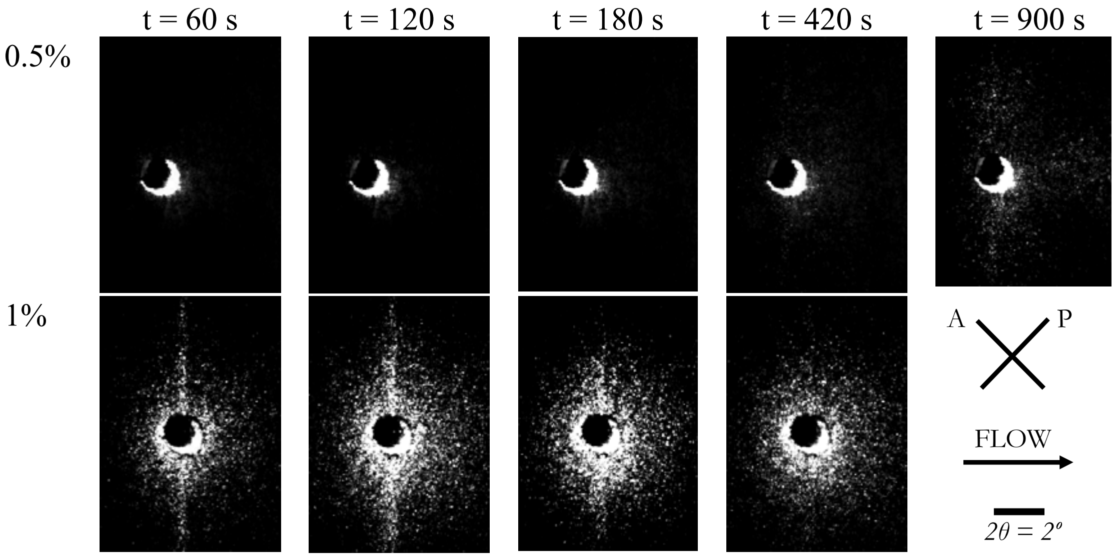

Figure 5.16 H_v SALS images collected subsequent to shear at 98 °C, $\sigma_w = 0.14$ MPa for t_s = 10 s.

5.3.2.2 X-ray Characterization

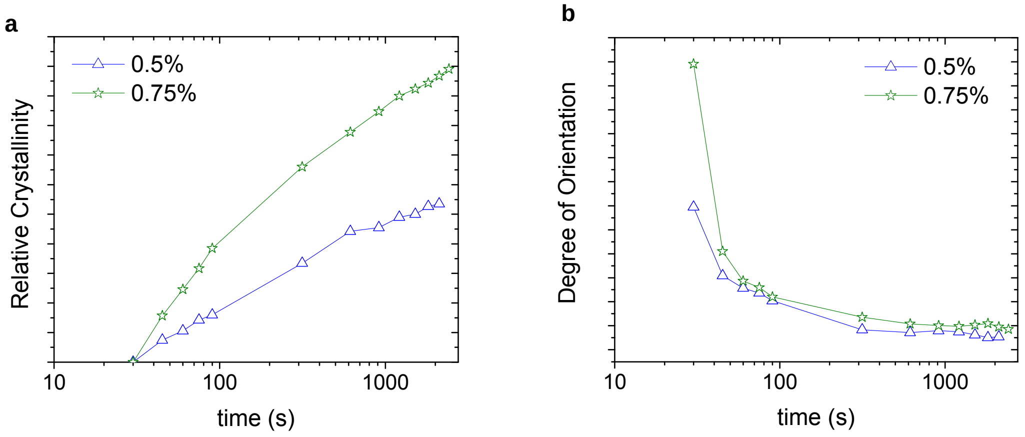

Figure 5.17 a) Relative crystallinity (measured as (110) peak intensity) and **b)** degree of orientation (measured as the second harmonic of Fourier transform of intensity versus azimuthal angle) for crystallization of HDPE subsequent to shear at 95 °C, $\sigma_w = 0.09$ MPa, $t_s = 15$ s.

The surprisingly low levels of oriented crystallization of these materials despite evidence that oriented precursors were formed during shear was apparent in x-ray scattering results. SAXS patterns did not exhibit significant anisotropy, in contrast to the oriented lobes in the SAXS patterns typically observed in highly crystalline systems following flow (not shown).[4, 39, 60-62] WAXS intensity also exhibited very little azimuthal dependence. Furthermore, the degree of orientation quickly decreased during the first minute of crystallization while crystallinity continued to increase (Figure 5.17).

5.4 DISCUSSION

5.4.1 Quiescent Crystallization

5.4.1.1 Nucleation Effects

High density polyethylene (HDPE) was found to serve as a nucleating agent in the ethylene-co-hexene (EH50) matrix, as has been similarly observed in other polyethylene systems.[28, 63] Enhanced crystallization kinetics were observed by DSC (Figure 5.4), optical transmittance (Figure 5.5), and x-ray scattering (Figure 5.13). At the concentrations examined ($c < 1$ wt % HDPE), an increase in HDPE concentration resulted in an increase in crystallization kinetics.[28, 64] Furthermore, this nucleation effect was insensitive to thermal history when the HDPE concentration was below overlap ($c < c^* \approx 0.6$ wt %), but was dependent on thermal history for blends having a concentration of HDPE that is above its overlap concentration ($c > c^*$).

In DSC nucleation studies, the 0.5 wt % blend ($c < c^* \approx 0.6$ wt %) exhibited little change in response to hold times of up to 5 min at both 105 and 100 °C. On the other hand, crystallization kinetics of the 1 wt % blend exhibited much stronger dependence on hold time at elevated temperatures. An order of magnitude decrease in peak crystallization time was observed following a hold of 3 min at 100 °C compared to t_{hold} = 0 min. At these intermediate temperatures, HDPE is highly supercooled (31 °C and 36 °C below the peak melting point of neat HDPE). On the other hand, neat EH50 is incapable of crystallization on short time scales (peak melting temperature 96 °C), and hence, crystal nuclei are predominantly composed of HPDE chains.

When the amount of HDPE is below the overlap concentration, crystallization of HPDE at intermediate temperatures of 100 and 105 °C is limited by the diffusion of HDPE chains to the growth front. This results in HDPE nucleating structures that are sparse, compact, and isolated; one can envision nucleated HDPE structures that are surrounded by region depleted of HDPE chains. On the other hand, at concentrations above overlap, HDPE crystals can readily propagate through the melt forming a network of nucleating structures. Overlap concentration of a slow-relaxing species is known to be important in bimodal systems undergoing flow-induced crystallization (FIC).[39, 65-68] In FIC, concentration of slow-relaxing species in a bimodal blend is important due to differences in melt dynamics, which dictate the response of the system to flow. However, to the best of our knowledge, this is the first time a non-linear concentration dependence of crystallization kinetics on a slow-relaxing species has been observed for quiescent crystallization; in fact, in contrast to observations here, iPP blends (which consist of components that are equally subcooled) exhibit nearly identical turbidity traces during isothermal crystallization, independent of whether high-molecular weight chains (slow-relaxing species) are above overlap or completely absent.[61] The difference in behavior observed here arises from the different degrees of subcooling for the two components examined here; under quiescent conditions, crystallization of the HDPE/EH50 blends is dictated by both the difference between the melting temperature of the two species and the diffusivity of the crystallizable chains. Therefore, systems utilizing a semicrystalline polymer as a nucleating agent are expected to exhibit a complex dependence on nucleant concentration, relative comonomer content, relative relaxation time, and thermal and flow histories.

5.4.1.2 Morphology Evolution

Neat EH50 was found to be incapable of multi-lamellar structure formation under the conditions examined. At 98 °C, it crystallized slowly (only after approximately 30 min), forming short, randomly oriented lamellae (Figure 5.14a). The lack of multi-lamellar structure was apparent from the isotropic H_v SALS patterns (Figure 5.6a).

The minima in optical transmittance curves (Figure 5.7) and the 4-lobe patterns in H_v SALS images exhibited by HDPE/EH50 blends (Figure 5.8) have previously been attributed to spherulite formation when observed during isothermal crystallization of polyethylene.[49, 50, 54] In past studies, the 4-lobe pattern in H_v scattering arose from the optical anisotropy of a polyethylene spherulite (resulting from different indices of refraction along the axes of the orthorhombic unit cell[69]).[52] The difference between the onset of the decrease in light transmittance and the onset of significant H_v scattering has been explained by a low level of anisotropy in the initial crystal structures, either as a consequence of low crystallinity or low orientation correlation among crystals.[49] The minimum in transmittance has been interpreted as the point at which spherulites fill 50% of the available volume as a consequence of the dependence of light scattering on the difference in the index of refraction and the amount of the scattering entities (spherulites) and the surrounding medium (melt).[49, 50, 54] Following this point, the transmittance increases due to the increasing size of the spherulites; an increase in size of scattering objects results in the contraction of the scattering pattern leading to more scattering at lower angles near 0°, and hence, more light entering the photodetector.[50] A difference in optical behavior between these previous studies and the present study is the transmittance following spherulite impingement. Here the transmittance values decline, whereas in the previous studies, transmittance stabilized at a constant value that corresponded to the orientation correlations (anisotropy) within the spherulite.[50] However, present materials are distinguished by the conspicuous absence of spherulitic structure when examined using either polarized light optical microscopy (POM), which would detect spherulites on lengths scales greater an a micron, or using electron microscopy, which would detect submicron-sized spherulites in these HDPE/EH50 blends (Figure 5.10b and Figure 5.14b).

Three-dimensional spherulites are not able to propagate at 95 or 98 °C due to the limited amount of crystallizable material (i.e., small concentrations of HDPE and limited number of ethylene sequences of sufficient length in EH50). Instead, we envision two-dimensional growth, or discs (Figure 5.18), which, when randomly oriented, also give a 4-lobe H_v scattering pattern.[70-72] The difference in the time between the onset of the drop in transmittance and the onset of H_v scattering can again be explained by low anisotropy of the initial scattering particles (Figure 5.18a). Likewise, the minimum in transmittance and the accompanying appearance of the 4-lobe pattern can be attributed to half-space-filling of the anisotropic, randomly-oriented, stacks of discs (Figure 5.18b). As the number of discs in a stack increases, the anisotropy of the system increases, resulting in an increase in H_v scattering.

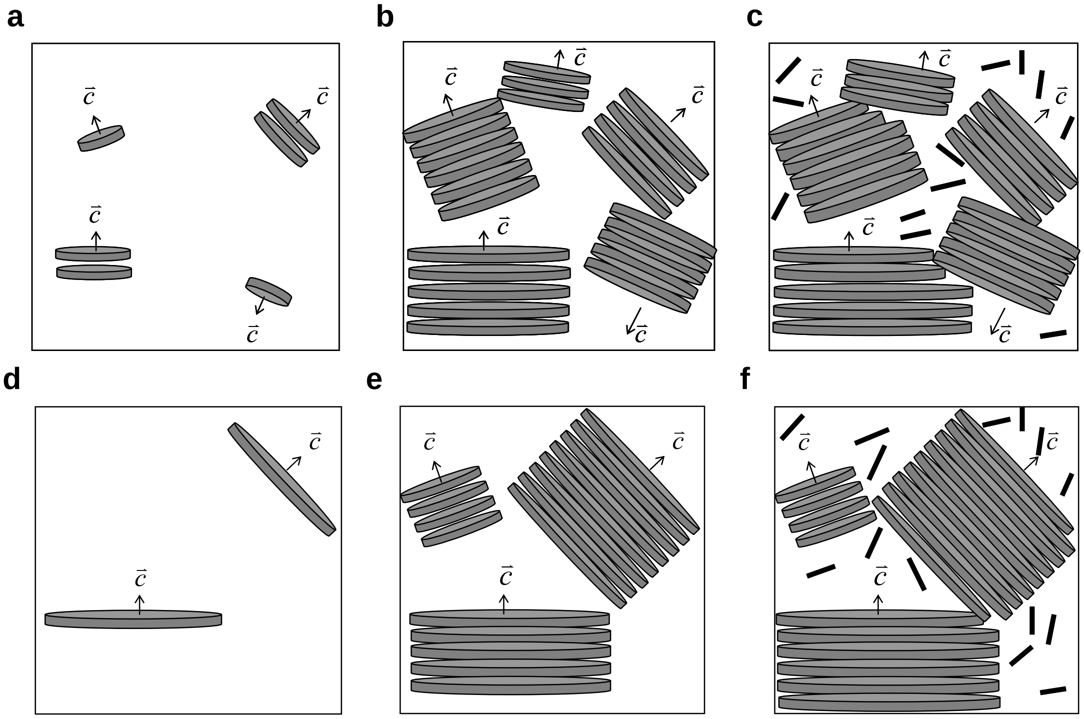

Figure 5.18 Schematic representation of isothermal crystallization of 0.5 and 1 wt % HDPE blends before the minimum in transmittance (**a** and **d**, respectively), after minimum in transmittance (**b** and **e**, respectively), and at long times when transmittance decreases (**c** and **f**, respectively). Vector c indicates direction of chain axis.

The presence of stacks, as indicated by high degree of local orientation in STEM micrographs (Figure 5.14b), is likely the consequence of HDPE templating, which has been previously observed under shear.[46, 68] In this scenario, the initial discs that form dictate the surrounding orientation distribution since only the crystal structures oriented roughly parallel to the initial discs can propagate. Similar to the case of spherulitic morphology, scattering at zero angle increases as the stacks of discs grow in size, resulting in an increase in transmittance. A constant value of transmittance is not reached at long times because total impingement of crystal structures is not achieved. Instead, transmittance decreases as H_v scattering increases both at and between the 'lobes,' consistent with the growth of randomly oriented lamellae that occur in neat EH50 (Figure 5.18c).

The HDPE/EH50 blend containing HDPE concentration above overlap ($c = 1$ wt % $> c^* \approx 0.6$ wt %) follows a similar evolution of a 4-lobe pattern as the 0.5 wt % blend ($c < c^*$) but starting from isotropic H_v scattering upon reaching $T_c = 98$ °C, which indicates crystallization of the blend during cooling. The fact that the initial scattering pattern is isotropic rather than 4-lobe means that the initial scattering entities are large but not arranged in stacks of discs. Instead, one can envision isolated, unilamellar discs, approximately 15 nm thick (from SAXS) and 1 μm in diameter, composed primarily of HPDE (Figure 5.18d). Since HDPE concentration is above overlap and chain diffusion limitations are reduced, HDPE chains can rapidly form nuclei and the growth front can advance more rapidly compared to the 0.5 wt % blend, resulting in crystallization during cooling (~8 °C/min). Hence, crystallization of the 1 wt % blend occurs at higher temperatures, leading to increased amounts of crystallization-induced phase separation. Although STEM images for the 1 wt % blend were not available, one can envision them to be intermediate between Figure 5.14b and Figure 5.14c, corresponding to the 0.5 and 5 wt % HDPE blends, respectively. Similar to the latter, the 1 wt % HDPE blend likely contains some large lamellae that do not template the surrounding crystallites; hence, they contribute to isotropic H_v scattering. However, the appearance of a 4-lobe H_v SALS pattern indicates that the 1 wt % HDPE blend still contains templated regions in which stacks of lamellar discs can be found (Figure 5.18 e and f).

Blends containing HDPE exhibited increased clarity with increasing HDPE content at long times during isothermal crystallization. Since the sample is contained between two windows, surface effects are negligible and the clarity is only a function of bulk optical transmittance. The clarifying effect of nucleating agents has been observed previously in spherulitic iPP systems, in which the clarifying effect was attributed to a decrease in spherulite size and a decrease in their scattering effectiveness with increasing nucleation density.[64] Highly crystalline systems, such as iPP and HPDE, are turbid due to large, closely-packed spherulites. EH50 has higher clarity than such highly crystalline systems because it does not organize into multi-lamellar structures. However, an intermediate amount of order, such as that in HDPE/EH50 blends, results in a further increase of sample clarity, which is important for the production of plastic films.[29]

5.4.2 Flow-Induced Crystallization

The interplay between defect-free HDPE chains and a defect-ridden copolymer matrix results in morphology evolution that is not commonly encountered in FIC of semicrystalline systems. Blends containing 0.5 and 1 wt % HDPE exhibited several unusual optical behaviors subsequent to flow (Figure 5.15a): (1) the transmittance of the 1 wt % HDPE blend increased during the shear pulse, (2) the transmittance at long times of the 1 wt % blend was lower for the sheared case than the quiescent case, while (3) the transmittance of the 0.5 wt % blend was higher compared with the quiescent case.

Initial crystal structures in both blends nucleate/template crystal growth at longer times. Flow can both alter the orientation distribution of structures formed during cooling and induce the formation of additional precursors. The orientation distribution of structures within the system at the cessation of flow will affect the orientation distribution of crystallites that propagate from the initial structures at later times. As mentioned previously, crystallization of the 1 wt % blend during cooling resulted in the formation of large crystals that were capable of scattering light (Figure 5.18d). Hence, the orientation of these large, platelet-like crystals by flow resulted in a strong increase in transmittance (the increase in transmittance was not the result of crystal destruction, as confirmed by WAXS—not shown). This behavior is reminiscent of increased transmittance following the elongation of polymer films.[50] In the present case, this increase in transmittance can be explained by the specific orientation of the platelet-shaped crystals by shear flow. In previous studies, platelet-like particles have been observed to be oriented such that their surface normal ($\vec{c}$ in Figure 5.19 corresponding to the chain axis) is nearly parallel to the velocity gradient direction ($\nabla \mathbf{v}$),[73-76] which in the current system corresponds to the direction of light through the sample (Figure 5.19). Prior to shear, the random orientation of discs results in scattering arising from the difference between refractive indices along the three unit cell axes (*a*, *b*, and *c* with refractive indices of 1.514, 1.519, and 1.575, respectively)[69] and the polyethylene melt (refractive index of approximately 1.49).[77] Subsequent to shear, the c-axis is aligned along the light path (Figure 5.19); hence, the contrast in refractive indices that is probed is reduced to 1.514 and 1.519 for the crystallites—quite close to that of the melt (1.49) so the transmittance increases.

Although an increase in transmittance is not observed during shear of the 0.5 wt % HDPE blend, DSC nucleation studies indicate that some structure formation in this blend is expected during cooling. However, at short crystallization times, these structures are too small to scatter light (Figure 5.18a). Evidence for their orientation is not apparent until long times when they have increased in size, resulting in increased transmittance of the sheared 0.5 wt % blend compared with the quiescent case.

In addition to orientation of pre-existing crystals, application of shear to the 1 wt % blend results in oriented nuclei formation (evident from apparent birefringence in

Figure 5.15b and streak in the H_v SALS pattern in Figure 5.16). Scattering from these cylindrical objects results in a large increase in turbidity of the sample due to the fact that their *c*-axis is oriented parallel to the direction of flow. This effect offsets the increase in transmittance from the orientation of pre-exiting platelet-like crystals resulting in a decrease in transmittance relative to the quiescent case of the 1 wt % HDPE blend.

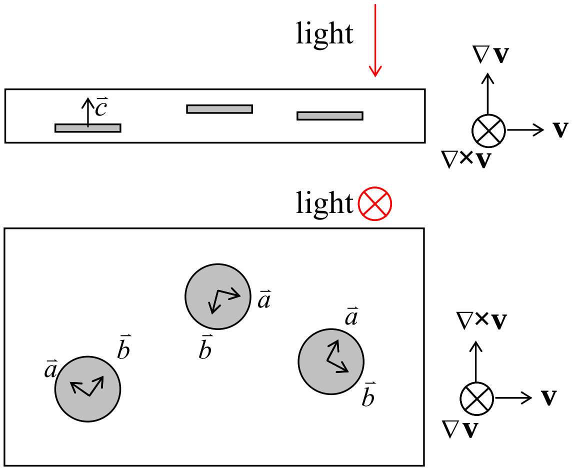

Figure 5.19 Schematic representation of orientation of lamellar discs by flow.

HDPE/EH50 blends did not exhibit the strong response to flow-induced crystallization (FIC) typical of more crystalline systems.[4, 39, 46, 60-62, 67, 78, 79] While this is expected at HDPE concentrations below overlap ($c < c^*$) where slow-relaxing species (here, HPDE chains) are not effective at triggering oriented nuclei formation,[65, 66, 80] it was surprising that 0.75 wt % and 1 wt % blends ($c > c^*$) also did not exhibit evidence of a dominant oriented morphology. Instead, the behavior of the latter blends suggests two crystallization regimes: (1) oriented structure propagation at short times following shear and (2) isotropic crystal growth at longer times.

At short times (t < 200 s), HDPE/EH50 blends exhibited evidence of oriented growth in the form of a rapidly increasing apparent birefringence trace that began from a non-zero value following shear (Figure 5.15b), a streak in the H_v scattering pattern (Figure 5.16), and an elevated degree of orientation in the WAXS images (Figure 5.17). Following 200 s, however, oriented growth appeared to have stopped. In contrast to more crystalline systems (see, for example, Figure B.3), the slope in I_{perp}/I dropped to a smaller, almost constant value. This change coincided with the poorly-defined minimum in the corresponding transmittance curve. A small increase in transmittance following the minimum is consistent with a lack of significant increase in the size of oriented structures. Further evidence that the growth front from the oriented precursors halts its advance is the absence of a contraction of the scattering patterns.[50, 81] Additionally, following the break in the rate of oriented growth, H_v SALS patterns developed significant isotropic scattering and the WAXS degree of orientation drastically decreased due to an increase in isotropic scattering.

The transition to isotropic scattering is a consequence of the copolymer base matrix. As oriented structures propagate, the longest ethylene sequences of EH50 are incorporated into the crystal. However, along with these crystallizable sequences, defects in the form of short-chain branches are also encountered. As more and more defects are crowded at the growth front, the crystal structures cease to grow and crystallization can only continue from newly-formed point-like nuclei in the melt. Therefore, the incorporation of the copolymer matrix into the oriented crystals pollutes the growth front, limiting the size of the oriented structures. This reasoning is similar to the explanation for the deterioration of morphology observed with increased SCB content of copolymers during quiescent crystallization.[19] Consequently, one could conjecture that the lateral dimensions of crystal structures can be manipulated by controlling the length of ethylene sequences consumed by the growth front (i.e., number of short-chain branches encountered), which, in turn, can be achieved by changing the temperature of crystallization (Figure 5.20).

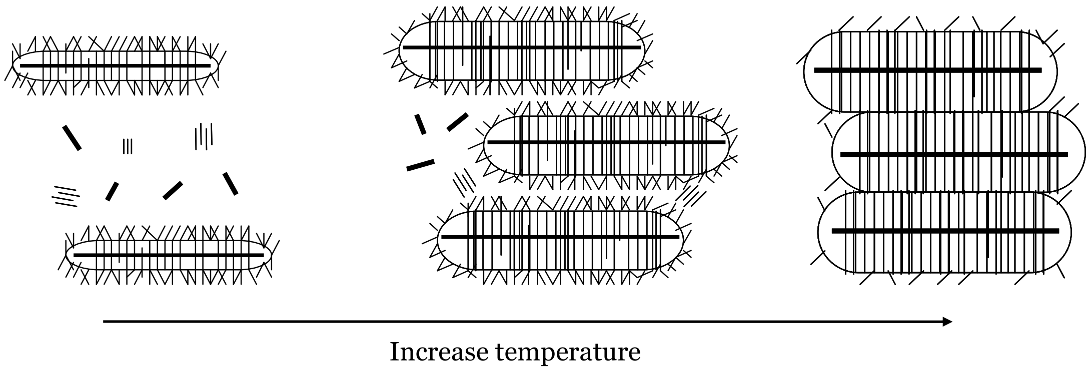

Figure 5.20 Schematic representation of the varying extent of oriented growth as a consequence of comonomer incorporation as dictated by temperature.

In agreement with this theory is the study by Hsiao et al. on bimodal blends composed of a linear ultrahigh molecular weight polyethylene (UHMWPE) at a low concentration (c = 2 wt % > c^*) in a short-chain-branched matrix.[82] This previous study revealed the propagation of large oriented shish-kebab structures following shear at elevated temperatures, at which the major, short-chain branched component could not crystallize.

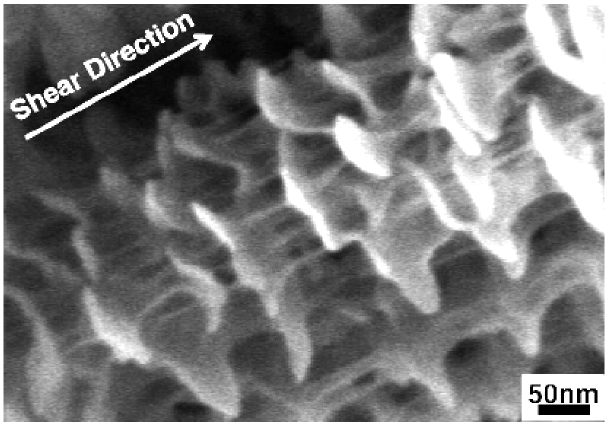

Figure 5.21 Shish-kebab structure observed subsequent to flow of a blend containing 2 wt % UHMWPE in a non-crystallizable PE. (Reprinted Fig. 3 with permission from Hsiao, B.S., et al. Phys. Rev. Lett. Vol. 94, 117802, 2005. Copyright (2005) by the American Physical Society).

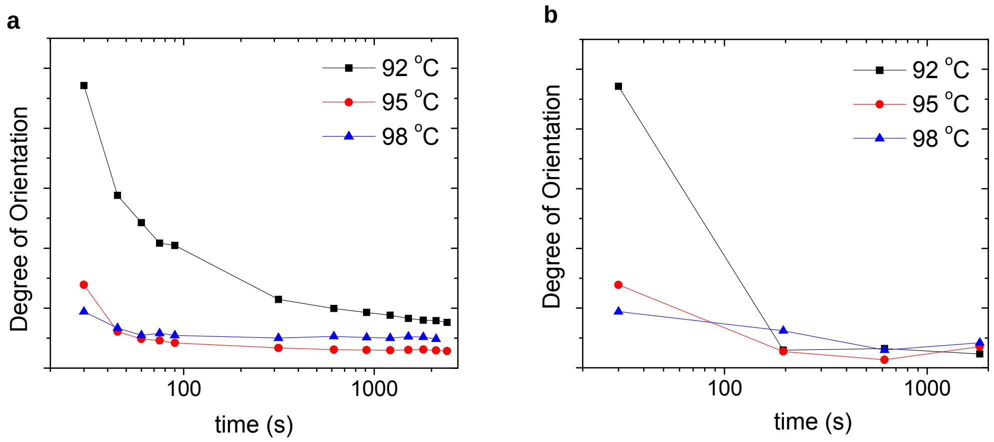

Figure 5.22 Evolution of degree of orientation of 0.75 wt % HDPE blend subsequent to shear at $\sigma_w = 0.09$ MPa for $t_s = 15$ s at different temperatures for **a)** full scattering patterns and **b)** differential scattering patterns.

Our theory was further confirmed by examining the degree of orientation of the 0.75 wt % blend at three different temperatures: 92, 95, and 98 °C (Figure 5.22a). The lowest temperature exhibited the greatest degree of orientation as more EH50 material could crystallize due the decrease in the required ethylene sequence length; only a small amount of orientation was evident at the highest crystallization temperature. For all three temperatures, a rapid decrease in WAXS anisotropy was observed. Further investigation into this evolution of WAXS anisotropy was conducted using the differential analysis developed by Hajimorad et al.[45] The relative degree of orientation was calculated for WAXS patterns that developed between the four time points of interest: (1) $0 < t_c < 30$ s, (2) $30 < t_c < 195$s, (3) $195 < t_c < 615$ s, and (4) $615 < t_c < 1815$ s. Crystallization occurring within 30 s of shear was characterized by the greatest degree of orientation (Figure 5.22b). At the two lower temperatures, 92 and 95 °C, anisotropy of subsequent crystallization (immediately following t = 30 s) was substantially diminished. In contrast, the anisotropy of crystallization at 98 °C was nearly constant from 0 to 195 s consistent with less pollution of the oriented growth front at the elevated temperature.

Not surprisingly, temperature affects more than simply the amount of EH50 that can crystallize. The large difference between the melting points of ethylene copolymers and branch-free PE chains, which are necessary to ensure formation of oriented nuclei, leads to a significant amount of material that is already crystalline upon reaching T_c in this system resulting in poor control of initial system morphology. In future work, a potential means to circumvent difficulties regarding oriented nuclei formation is to utilize a system with embedded oriented fibers that can serve as well controlled (size and amount) oriented nuclei. This will allow one to utilize instruments having better temperature control which are not limited by large thermal mass. Rapid cooling in addition to examination of materials having slightly less comonomer content may decrease crystallization-induced phase separation and allow for proper control of the initial morphology.

5.5 CONCLUSION

Crystallization of an ethylene-copolymer (EH50) was examined in the presence of small concentrations ($c < 5$ wt %) of a high density polyethylene (HDPE) both under quiescent conditions and subsequent to flow at temperatures where both blend components could crystallize. These multimodal systems may be encountered in industry both by specific blending and through specific synthetic routes to metallocene copolymers. Due to the difference in melting point between the two materials as a consequence of short-chain branching, HDPE proved to be an effective nucleating agent. Furthermore, due to its semicrystalline nature and its ability to organize into super molecular structures, the effectiveness of HDPE as a nucleant was found to be sensitive to thermal history above its overlap concentration ($c > c^*$).

HDPE also proved to be an effective clarifying agent. Small concentrations ($c <$ 1 wt %) of HDPE resulted in high clarity samples at long crystallization times. This was a consequence of a change in morphology from randomly distributed lamellae (without HDPE) to stacks of lamellae having local orientation (with small amounts of HDPE). The clarifying effect was evident both under isothermal conditions and subsequent to shear.

HDPE/EH50 blends containing 1 wt % HDPE or less exhibited surprisingly little response to shear in contrast to more crystalline isotactic polypropylene (iPP) and HDPE systems. Evidence of a dominant oriented morphology was not observed. Instead, the samples exhibited two crystallization regimes: (1) oriented growth at short times following shear and (2) isotropic growth at long times following shear. The transition between the two regimes appears to be a consequence of the incorporation of ethylene sequences into the oriented structures which results in a build up of short-chain branches (i.e., defects) and a pollution of the growth front. At later times, the oriented growth front is extinguished by the tethered copolymer. Subsequent growth requires new nuclei to form; since the remaining melt is fully relaxed at these long times, point-like nuclei form and the subsequent growth is isotropic.

We propose that this behavior can be exploited to control the lateral dimensions of the oriented structures by controlling the incorporation of ethylene sequences, which, in turn, is dictated by temperature. The ability to precisely control the size of morphological features in semicrystalline systems would enable more accurate tuning of the ultimate physical properties.

5.6 ACKNOWLEDGEMENTS

This work would not have been possible without ExxonMobil Research and Engineering Company, particularly Dr. David Lohse, Dr. Manika Varma-Nair, Dr. Andrew Tsou and the rest of the team, who provided materials, financial support, experimental assistance, and fruitful discussions. Additionally, we thank Dr. John Stuyver and Dr. Anton-Jan Bons (ExxonMobil, Machelen, Belgium) for providing STEM images. We would like to thank Dr. Soo-Young Park (Kyunpook National University, Daegu, South Korea) for conducting DSC studies. We must thank the beamline staff at beamline X27C at NSLS BNL (Dr. Lixia Rong and Jie Zhu) and BM26 DUBBLE at ESRF (Dr. Wim Bras, Dr. Kristina Kvanshnina, Dr. Giuseppe Portale, and Dirk Detollenaere). X-ray scattering experiments were conducted with the help of Dr. Lucia Fernandez Ballester (ESRF, DUBBLE, Grenoble, France), Dr. Timothy Gough (University of Bradford, UK), Dr. Fernando Ania, and Dr. Araceli Flores (Instituto de Estructura de la Materia, Madrid, Spain). Part of this work was also funded by the National Science Foundation (DMR-0505393 and GOALI-0523083). Manuscript preparation was aided by Prof. Julia Kornfield and Mary Louie (Caltech).

5.7 REFERENCES

1. Mirabella, F. M., Correlation of the melting behavior and copolymer composition distribution of Ziegler-Natta-catalyst and single-site-catalyst polyethylene copolymers. *Journal of Polymer Science Part B-Polymer Physics* **2001,** 39, (22), 2800-2818.
2. Galante, M. J.; Mandelkern, L.; Alamo, R. G.; Lehtinen, A.; Paukkeri, R., Crystallization kinetics of metallocene type polypropylenes - Influence of molecular weight and comparison with Ziegler-Natta type systems. *Journal of Thermal Analysis* **1996,** 47, (4), 913-929.
3. Malmberg, A.; Kokko, E.; Lehmus, P.; Lofgren, B.; Seppala, J. V., Long-chain branched polyethene polymerized by metallocene catalysts Et[Ind](2)ZrCl2/MAO and Et[IndH(4)](2)ZrCl2/MAO. *Macromolecules* **1998,** 31, (24), 8448-8454.
4. Agarwal, P. K.; Somani, R. H.; Weng, W.; Mehta, A.; Yang, L.; Ran, S.; Liu, L.; Hsiao, B. S., Shear-Induced Crystallization in Novel Long Chain Branched Polypropylenes by in Sity Rheo-SAXS and -WAXD. *Macromolecules* **2003,** 36, 5226-5235.
5. Shiono, T.; Azad, S. M.; Ikeda, T., Copolymerization of atactic polypropene macromonomer with propene by an isospecific metallocene catalyst. *Macromolecules* **1999,** 32, (18), 5723-5727.
6. Mehdiabadi, S.; Soares, J. B. P.; Dekmezian, A. H., Production of Long-Chain Branched Polyolefins with Two Single-Site Catalysts: Comparing CSTR and Semi-Batch Performance. *Macromolecular Reaction Engineering* **2008,** 2, (6), 529-550.
7. Schwerdtfeger, E. D.; Irwin, L. J.; Miller, S. A., Highly branched polyethylene from ethylene alone via a single zirconium-based catalyst. *Macromolecules* **2008,** 41, (4), 1080-1085.
8. Lofgren, B.; Kokko, E.; Seppala, J., Specific structures enabled by metallocene catalysis in polyethenes. In *Long-Term Properties of Polyolefins*, Springer-Verlag Ber-

lin: Berlin, 2004; Vol. 169, pp 1-12.

9. Wang, C.; Chu, M. C.; Lin, T. L.; Lai, S. M.; Shih, H. H.; Yang, J. C., Microstructures of a highly short-chain branched polyethylene. *Polymer* **2001,** 42, (4), 1733-1741.
10. Chiu, F. C.; Wang, Q.; Fu, Q.; Honigfort, P.; Cheng, S. Z. D.; Hsiao, B. S.; Yeh, F. J.; Keating, M. Y.; Hsieh, E. T.; Tso, C. C., Structural and morphological inhomogeneity of short-chain branched polyethylenes in multiple-step crystallization. *Journal of Macromolecular Science-Physics* **2000,** B39, (3), 317-331.
11. Zhang, F. J.; Liu, J. P.; Xie, F. C.; Fu, Q.; He, T. B., Polydispersity of ethylene sequence length in metallocene ethylene/alpha-olefin copolymers. II. Influence on crystallization and melting behavior. *Journal of Polymer Science Part B-Polymer Physics* **2002,** 40, (9), 822-830.
12. Xu, J. T.; Li, B. T.; Fan, Z. Q.; Ryan, A. J., Simultaneous SAXS/WAXS/DSC studies on microstructure of conventional and metallocene-based ethylene-butene copolymers. *Chinese Journal of Polymer Science* **2004,** 22, (3), 279-287.
13. Perez, E.; Benavente, R.; Quijada, R.; Narvaez, A.; Galland, G. B., Structure characterization of copolymers of ethylene and 1-octadecene. *Journal of Polymer Science Part B-Polymer Physics* **2000,** 38, (11), 1440-1448.
14. Stadler, F. J.; Takahashi, T.; Yonetake, K., Crystallite dimensions - characterization of ethene-/alpha-olefin Copolymers with various comonomers and comonomer Ccontents measured by small- and wide angle X-ray scattering. *E-Polymers* **2009**, 19.
15. Bubeck, R. A., Structure-property relationships in metallocene polyethylenes. *Materials Science and Engineering R* **2002,** 39, 1-28.
16. Cerrada, M. L.; Benavente, R.; Perez, E., Influence of thermal history on morphology and viscoelastic behavior of ethylene-1-octene copolymers synthesized with metallocene catalysts. *Journal of Materials Research* **2001,** 16, (4), 1103-1111.

17. Peeters, M.; Goderis, B.; Vonk, C.; Reynaers, H.; Mathot, V., Morphology of Homogeneous Copolymers of Ethene and 1-Octene. I. Influence of Thermal History on Morphology. *Journal of Polymer Science: Part B: Polymer Physics* **1997,** 35, 2689-2713.
18. Krishnaswamy, R. K.; Yang, Q.; Fernandez-Ballester, L.; Kornfield, J. A., Effect of the distribution of short-chain branches on crystallization kinetics and mechanical properties of high-density polyethylene. *Macromolecules* **2008,** 41, (5), 1693-1704.
19. Bensason, S.; Minick, J.; Moet, A.; Chum, S.; Hiltner, A.; Baer, E., Classification of Homogeneous Ethylene-Octene Copolymers Based on Comonomer Content. *Journal of Polymer Science: Part B: Polymer Physics* **1996,** 34, 1301-1315.
20. Alamo, R.; Domszy, R.; Mandelkern, L., Thermodynamic and Structural-Properties of Copolymers of Ethylene. *Journal of Physical Chemistry* **1984,** 88, (26), 6587-6595.
21. Alamo, R. G.; Viers, B. D.; Mandelkern, L., Phase-Structure of Random Ethylene Copolymers - a Study of Counit Content and Molecular-Weight as Independent Variables. *Macromolecules* **1993,** 26, (21), 5740-5747.
22. Alizadeh, A.; Richardson, L.; Xu, J.; McCartney, S.; Marand, H.; Cheung, Y. W.; Chum, S., Influence of Structural and Topological Constraints on the Crystallization and Melting Behavior of Polymers. 1. Ethylene/1-Octene Copolymers. *Macromolecues* **1999,** 32, 6221-6235.
23. Richardson, M. J.; Flory, P. J.; Jackson, J. B., Crystallization and Melting of Copolymers of Polymethylene. *Polymer* **1963,** 4, (2), 221-236.
24. Alamo, R. G.; Mandelkern, L., Thermodynamic and Structural-Properties of Ethylene Copolymers. *Macromolecules* **1989,** 22, (3), 1273-1277.
25. Adhikari, R.; Godehardt, R.; Lebek, W.; Frangov, S.; Michler, G. H.; Radusch, H.; Calleja, F. J. B. In *Morphology and micromechanical properties of ethylene/1-octene copolymers and their blends with high density polyethylene*, 2005; John Wiley &

Sons Ltd: 2005; pp 156-166.

26. Adhikari, R.; Godehardt, R.; Lebek, W.; Michler, G. H., Blends of High Density Polyethylene and Ethylene/1-Octene Copolymers: Structure and Properties. *Journal of Applied Polymer Science* **2007,** 103, 1887-1893.
27. Bensason, S.; Nazarenko, S.; Chum, S.; Hiltner, A.; Baer, E., Blends of homogeneous ethylene-octene copolymers. *Polymer* **1997,** 38, (14), 3513-3520.
28. Song, S. J.; Wu, P. Y.; Ye, M. X.; Feng, J. C.; Yang, Y. L., Effect of small amount of ultra high molecular weight component on the crystallization behaviors of bimodal high density polyethylene. *Polymer* **2008,** 49, (12), 2964-2973.
29. Ommundsen, E.; Skar, M.; Nord-Varhaug, K. Nucleating Agent. 2007.
30. Andreassen, E.; Larsen, A.; Nord-Varhaug, K.; Skar, M.; Oysaed, H., Haze of Polyethylene Films -- Effects of Material Parameters and Clafifying Agents. *Polymer Engineering and Science* **2002,** 42, (5), 1082-1097.
31. Rubinstein, M.; Colby, R. H., *Polymer Physics*. Oxford University Press: New York, 2003.
32. Nogales, A.; Hsiao, B. S.; Somani, R. H.; Srinivas, S.; Tsou, A. H.; Balta-Calleja, F. J.; Ezquerra, T. A., Shear-induced crystallization of isotactic polypropylene with different molecular weight distributions: in situ small- and wide-angle X-ray scattering studies. *Polymer* **2001,** 42, (12), 5247-5256.
33. deGennes, P.-G., *Scaling Concepts in Polymer Physics*. Cornell University Press: Ithica, NY, 1979.
34. Takahashi, Y.; Isono, Y.; Noda, I.; Nagasawa, M., Zero-Shear Viscosity of Linear Polymer Solutions over a Wide Range of Concentration. *Macromolecules* **1985,** 18, (5), 1002-1008.
35. Schelten, J.; Ballard, D. G. H.; Wignall, G. D.; Longman, G.; Schmatz, W., Small-Angle Neutron-Scattering Studies of Molten and Crystalline Polyethylene. *Polymer*

1976, 17, (9), 751-757.

36. Lieser, G.; Fischer, E. W.; Ibel, K., Conformation of Polyethylene Molecules in Melt as Revealed by Small-Angle Neutron-Scattering. *Journal of Polymer Science Part C-Polymer Letters* **1975,** 13, (1), 39-43.
37. Kumaraswamy, G.; Verma, R. K.; Kornfield, J. A., Novel flow apparatus for investigating shear-enhanced crystallization and structure development in semicrystalline polymers. *Review of Scientific Instruments* **1999,** 70, (4), 2097-2104.
38. Liedauer, S.; Eder, G.; Janeschitz-Kriegl, H.; Jerschow, P.; Geymayer, W.; Ingolic, E., On the kinetics of shear-induced crystallization in polypropylene. *International Polymer Processing* **1993,** 8, (3), 236-244.
39. Keum, J. K.; Zuo, F.; Hsiao, B. S., Probing the flow-induced shish-kebab structure in entangled polyethylene melts by synchrotron X-ray scattering. *Journal of Applied Crystallography* **2007,** 40, (Supplement), s48-s51.
40. Macosko, C. W., *Rheology: Principles, Measurements, and Applications*. VCH: New York, 1994.
41. The author would like to thank Dr. Lixia Rong and Jie Zhu with beamline assistance. Additionally, the author thanks Dr. Lucia Fernandez Ballester and Dr. Timothy Gough for experimental assistance.
42. The athor would like to thank beamline staff Dr. Wim Bras, Dr. Kristina Kvanshnina, Dr. Giuseppe Portale, and Dirk Detollenaere among others for their support. Additional experimental assistance was provided by Dr. Lucia Fernandez Ballester, Dr. Timothy Gough , Dr. Fernando Ania, and Dr. Araceli Flores.
43. Cser, F., About the Lorentz correction used in the interpretation of small angle X-ray scattering data of semicrystalline polymers. *Journal of Applied Polymer Science* **2001,** 80, (12), 2300-2308.
44. Aggarwal, S. L.; Tilley, G. P., Determination of Crystallinity in Polyethylene by X-

Ray Diffractometer. *Journal of Polymer Science* **1955,** 18, (87), 17-26.

45. Hajimorad, M.; Smirnova, D.; Kornfield, J., *Manuscript in preparation.* **2009**.
46. Langouche, F., Orientation deveopment during shear flow-induced crystallization of i-PP. *Macromolecules* **2006,** 39, 2568-2573.
47. Baert, J.; Van Puyvelde, P.; Langouche, F., Flow-induced crystallization of PB-1: From the low shear rate region up to processing rates. *Macromolecules* **2006,** 39, (26), 9215-9222.
48. Ding, Z. M.; Spruiell, J. E., An experimental method for studying nonisothermal crystallization of polymers at very high cooling rates. *Journal of Polymer Science Part B-Polymer Physics* **1996,** 34, (16), 2783-2804.
49. Akpalu, Y.; Kielhorn, L.; Hsiao, B. S.; Stein, R. S.; Russell, T. P.; Egmond, J. v.; Muthukumar, M., Structure Development during Crystallization of Homogeneous Copolymers of Ethene and 1-Octene: Time-Resolved Synchrotron X-ray and SALS Measurements. *Macromolecules* **1999,** 32, 765-770.
50. Clough, S.; Rhodes, M. B.; Stein, R. S., Transmission of Light by Films of Crystalline Polymers. *Journal of Polymer Science Part C-Polymer Symposium* **1967**, (18PC), 1-&.
51. Haudin, J. M., *Optical Properties of Polymers*. Elsevier Applied Science Publishers: New York, 1986.
52. Stein, R. S.; Rhodes, M. B., Photographic Light Scattering by Polyethylene Films. *Journal of Applied Physics* **1960,** 31, (11), 1873-1884.
53. Mandelkern, L.; Glotin, M.; Benson, R. A., Supermolecular Structure and Thermodynamic Properties of Linear and Branched Polyethylene under Rapid Crystallization Conditions. *Macromolecules* **1981,** 14, 22-34.
54. Xiao, Z. C.; Akpalu, Y. A., New insights into the characteristics of early stage crystallization of a polyethylene. *Polymer* **2007,** 48, (18), 5388-5397.

55. Kumaraswamy, G.; Kornfield, J. A.; Yeh, F.; Hsiao, B. S., Shear-Enhanced Crystallization in Isotatctic Polypropylene. 3. Evidence for a Kinetic Pathway to Nucleation. *Macromolecules* **2002,** 35, 1762-1769.
56. Kumaraswamy, G.; Issaian, A. M.; Kornfield, J. A., Shear-Enhanced Crystallization in Isotactic Polypropylene. 1. Correspondence between in Situ Rheo-Optics and ex Situ Structure Determination. *Macromolecules* **1999,** 32, (22), 7537-7547.
57. Jerschow, P.; Janeschitz-Kriegl, H., The role of long molecules and nucleating agents in shear induced crystallization of isotactic polypropylenes. *Internation Polymer Processing* **1997,** 12, (1), 72-77.
58. Pogodina, N. V.; Lavrenko, V. P.; Srinivas, S.; Winter, H. H., Rheology and structure of isotactic polypropylene near the gel point: quiescent and shear-induced crystallization. *Polymer* **2001,** 42, (21), 9031-9043.
59. Ogino, Y.; Fukushima, H.; Takahashi, N.; Matsuba, G.; Nishida, K.; Kanaya, T., Crystallization of Isotactice Polypropylene under Shear Flow Observed in a Wide Spatial Scale. *Macromolecules* **2006,** 39, 7617-7625.
60. Kumaraswamy, G.; Verma, R. K.; Kornfield, J. A.; Yeh, F.; Hsiao, B. S., Shear-enhanced crystallization in isotactic polypropylene. In-situ synchrotron SAXS and WAXD. *Macromolecules* **2004,** 37, 9005-9017.
61. Fernandez-Ballester, L. Formation of oriented precursors in flow-induced polymer crystallization: experimental methods and model materials. California Institute of Technology, Pasadena, CA, 2007.
62. Somani, R. H.; Hsiao, B. S.; Nogales, A.; Srinivas, S.; Tsou, A. H.; Sics, I.; Balta-Calleja, F. J.; Ezquerra, T. A., Structure Development during Shear Flow-Induced Crystallization of i-PP: In-Situ Small-Angle X-ray Scattering Study. *Macromolecules* **2000,** 33, 9385-9394.
63. Wendt, U., Nucleation of Low-Density Polyethylene by High-Density Polyethylene.

Journal of Materials Science Letters **1988,** 7, (6), 643-645.

64. Kristiansen, M.; Werner, M.; Tervoort, T.; Smith, P.; Blomenhofer, M.; Schmidt, H. W., The binary system isotactic polypropylene/bis(3,4-dimethylbenzylidene)sorbitol: Phase behavior, nucleation, and optical properties. *Macromolecules* **2003,** 36, (14), 5150-5156.
65. Seki, M.; Thurman, D. W.; Oberhauser, J. P.; Kornfield, J. A., Shear-mediated crystallization of isotatctic polypropylene: The role of long chain -- long chain overlap. *Macromolecules* **2002,** 35, 2583-2594.
66. Heeley, E. L.; Fernyhough, C. M.; Graham, R. S.; Olmsted, P. D.; Inkson, N. J.; Embery, J.; Groves, D. J.; McLeish, T. C. B.; Morgovan, A. C.; Meneau, F.; Bras, W.; Ryan, A. J., Shear-induced crystallization in blends of model linear and long-chain branched hydrogenated polybutadienes. *Macromolecules* **2006,** 39, 5058-5071.
67. Ogino, Y.; Fukushima, H.; Matsuba, G.; Takahashi, N.; Nishida, K.; Kanaya, T., Effects of high molecular weight component on crystallization of polyethylene under shear flow. *Polymer* **2006,** 47, 5669-5677.
68. Yang, L.; Somani, R. H.; Sics, I.; Hsiao, B. S.; Kolb, R.; Fruitwala, H.; Ong, C., Shear-induced crystallization precursor studies in model polyethylene blends by in-situ rheo-SAXS and rheo-WAXD. *Macromolecules* **2004,** 37, 4845-4859.
69. Bunn, C. W.; Daubeny, R. D., The Polarizabilities of Carbon Carbon Bonds. *Transactions of the Faraday Society* **1954,** 50, (11), 1173-1177.
70. Chu, W.; Stein, R. S., Effect of Birefringence on Low-Angle Light-Scattering Patterns from Oriented Polymer Films .2. *Journal of Polymer Science Part a-2-Polymer Physics* **1970,** 8, (4), 489-&.
71. Clough, S.; Vanaarts.J; Stein, R. S., Scattering of Light by 2-Dimensional Spherulites. *Journal of Applied Physics* **1965,** 36, (10), 3072-&.
72. Finkelst.Rs; Sarko, A., Light-Scattering by Anisotropic Elliptical Objects. *Journal of*

Polymer Science Part a-2-Polymer Physics **1972,** 10, (7), 1193-&.

73. Stefanescu, E. A.; Dundigalla, A.; Ferreiro, V.; Loizou, E.; Porcar, L.; Negulescu, I.; Garno, J.; Schmidt, G., Supramolecular structures in nanocomposite multilayered films. *Physical Chemistry Chemical Physics* **2006,** 8, (14), 1739-1746.
74. Bafna, A.; Beaucage, G.; Mirabella, F.; Mehta, S., 3D Hierarchical orientation in polymer-clay nanocomposite films. *Polymer* **2003,** 44, (4), 1103-1115.
75. Galgali, G.; Agarwal, S.; Lele, A., Effect of clay orientation on the tensile modulus of polypropylene-nanoclay composites. *Polymer* **2004,** 45, (17), 6059-6069.
76. Medellin-Rodriguez, F. J.; Burger, C.; Hsiao, B. S.; Chu, B.; Vaia, R.; Phillips, S., Time-resolved shear behavior of end-tethered Nylon 6-clay nanocomposites followed by non-isothermal crystallization. *Polymer* **2001,** 42, (21), 9015-9023.
77. Wiley Database of Polymer Properties. In John Wiley & Sons, Inc.: 1999-2009.
78. Yang, L.; Somani, R. H.; Sics, I.; Hsiao, B. S.; Kolb, R.; Lohse, D., The role of high molecular weight chains in flow-induced crystallization precursor structures. *Journal of Physics: Condensed Matter* **2006,** 18, S2421-S2436.
79. Pople, J. A.; Mitchell, G. R.; Sutton, S. J.; Vaughan, A. S.; Chai, C. K., The development of organized structures in polyethylene crystallized from a sheared melt, analyzed by WAXS and TEM. *Polymer* **1999,** 40, (10), 2769-2777.
80. Kumaraswamy, G., Crystallization of Polymers from Stressed Melts. *Journal of Macromolecular Science, Part C: Polymer Reviews* **2005,** 45, 375-397.
81. Ashizawa, H.; Spruiell, J. E.; White, J. L., An Investigation of Optical Clarity and Crystalline Orientation in Polyethylene Tubular Film. *Polymer Engineering and Science* **1984,** 24, (13), 1035-1042.
82. Hsiao, B. S.; Yang, L.; Somani, R. H.; Avila-Orta, C. A.; Zhu, L., Unexpected Shish-Kebab Structure in a Sheared Polyethylene Melt. *Physical Review Letters* **2005,** 94, (11).